EVOLUTIONARY BIOLOGY

High-performance suction feeding in an early elasmobranch

Michael I. Coates[1]*, Kristen Tietjen[1], Aaron M. Olsen[2], John A. Finarelli[3]

High-performance suction feeding is often presented as a classic innovation of ray-finned fishes, likely contributing to their remarkable evolutionary success, whereas sharks, with seemingly less sophisticated jaws, are generally portrayed as morphologically conservative throughout their history. Here, using a combination of computational modeling, physical modeling, and quantitative three-dimensional motion simulation, we analyze the cranial skeleton of one of the earliest known stem elasmobranchs, *Tristychius arcuatus* from the Middle Mississippian of Scotland. The feeding apparatus is revealed as highly derived, capable of substantial oral expansion, and with clear potential for high-performance suction feeding some 50 million years before the earliest osteichthyan equivalent. This exceptional jaw performance is not apparent from standard measures of ecomorphospace using two-dimensional data. *Tristychius* signals the emergence of entirely new chondrichthyan ecomorphologies in the aftermath of the end-Devonian extinction and highlights sharks as significant innovators in the early radiation of the modern vertebrate biota.

INTRODUCTION

Suction feeding is ubiquitous among aquatic vertebrates (*1*) and likely emerged in the earliest fishes (*2*). Improvements in efficiency advanced with the evolution of stiff jaws and hyoid arches, as well as powerful opening and closing mechanisms. However, true high-performance suction feeding required additional skeletal elements to occlude the corners of the mouth (*2*, *3*) and an independently rotating hyoid bar (ceratohyal and basihyal). These characteristics, often linked to the profound evolutionary radiation of ray-finned fishes (*4*, *5*), allow greater control over gape and buccal volume and are thought to have first evolved in the late Paleozoic in stem neopterygians (*6*). Nevertheless, similar mechanisms are also present in living elasmobranchs, most notably in the Orectolobiformes (*7*). Furthermore, the presence of labial cartilages in a variety of fossil forms (*8*, *9*) suggests an earlier origin, supporting the conjecture that high-performance suction feeding was first elaborated in the Chondrichthyes rather than the Osteichthyes (*2*).

Here, we combine new fossil data with kinematic simulations from digital and physical models to test this Chondrichthyes-first conjecture and quantitatively investigate whether these jaw functions evolved first within the early Carboniferous chondrichthyan radiation (*5*, *10*). *Tristychius arcuatus* (*11*), from the Middle Mississippian of Scotland (Fig. 1) (*12*, *13*), is known in almost complete skeletal detail from numerous specimens preserved in ironstone concretions from the Viséan (Asbian) Wardie Beach locality of Edinburgh, Scotland (figs. S1 to S3 and table S1) (*14*, *15*). Computed x-ray tomography of these concretions has already revealed new information about the braincase (Fig. 1, A to D) (*13*), confirming hypotheses (*12*, *16*, *17*) that *Tristychius* is a stem elasmobranch (Fig. 1E). These neurocranial data (*13*) provide new information about the arrangement of articulation areas for the jaws and jaw suspension, as well as details of the ear capsule and vestibular labyrinth, which indicate that *Tristychius* was capable of phonoreception and likely had benthic life habits (consistent with existing body reconstructions) (*12*). Additional information provided here about the three-dimensional (3D) morphology of the jaws, hyoid arch, and labial cartilages reveals structural and functional features formerly known only from more derived members of the elasmobranch clade (figs. S4 and S5) (*8*).

[1]Department of Organismal Biology and Anatomy, University of Chicago, 1027 E 57th St., Chicago, IL 60637, USA. [2]Department of Ecology and Evolutionary Biology, Brown University, 171 Meeting St., Box G-B 204, Providence, RI 02912, USA. [3]UCD School of Biology and Environmental Science, UCD Science Education and Research Centre (West), UCD Earth Institute, University College Dublin, Belfield, Dublin 4, Ireland.
*Corresponding author. Email: mcoates@uchicago.edu

RESULTS

Morphology

The jaws of *Tristychius* (Fig. 2, A to C, G, and I) differ in numerous respects from the standard jaw morphology found in most Paleozoic chondrichthyans (Fig. 2, D to F and H) (*8*, *18*). The "cleaver-shaped" (*19*) palatoquadrate is absent, and there is no lateral crest (*16*) marking the anterior boundary of an adductor fossa. Rather, the quadratomandibularis muscle occupied a suborbital location, extending anteriorly and, perhaps, onto the postnasal lamina. Dorsally, the quadrate region bears a unique transverse ridge-and-groove articulation (*8*) with the ventral surface of the postorbital process (Fig. 1C and fig. S4). The lateral and ventral extremity of the quadrate, likely derived from the otic process rim of other Paleozoic sharks, encloses the adductor fossa to the rear (Fig. 1D). The jaw joint, ventral to the postorbital process, is a close-fitting dual joint and conforms to the classic chondrichthyan medial and lateral ball and socket articulation (*20*). The lateral joint is ellipsoidal with a laterally directed long axis (fig. S2F), perpendicular to the longitudinal axis of the body, thus restricting jaw movement at the quadratomandibular articulation to a simple hinge (*21*). The spatulate anterior of the palatine process almost meets its counterpart but, unlike modern elasmobranchs (*3*), lacks a symphysial articulation. A small ethmoid process (fig. S2, B and C) marks the ligamentous connection with the braincase.

Meckel's cartilage is slender and elongate (fig. S2), with a lateral depression for the ventral division of the quadratomandibularis muscle. Most distinctively, an unusually large retroarticular process, ~12% of total mandibular length (Fig. 1C), engages with the recessed lateral surface of the proximal head of the ceratohyal (figs. S3E and S4). A similar arrangement occurs in modern orectolobiform sharks (fig. S5, B and C) (*3*, *7*, *22*) but with a much less prominent retroarticular

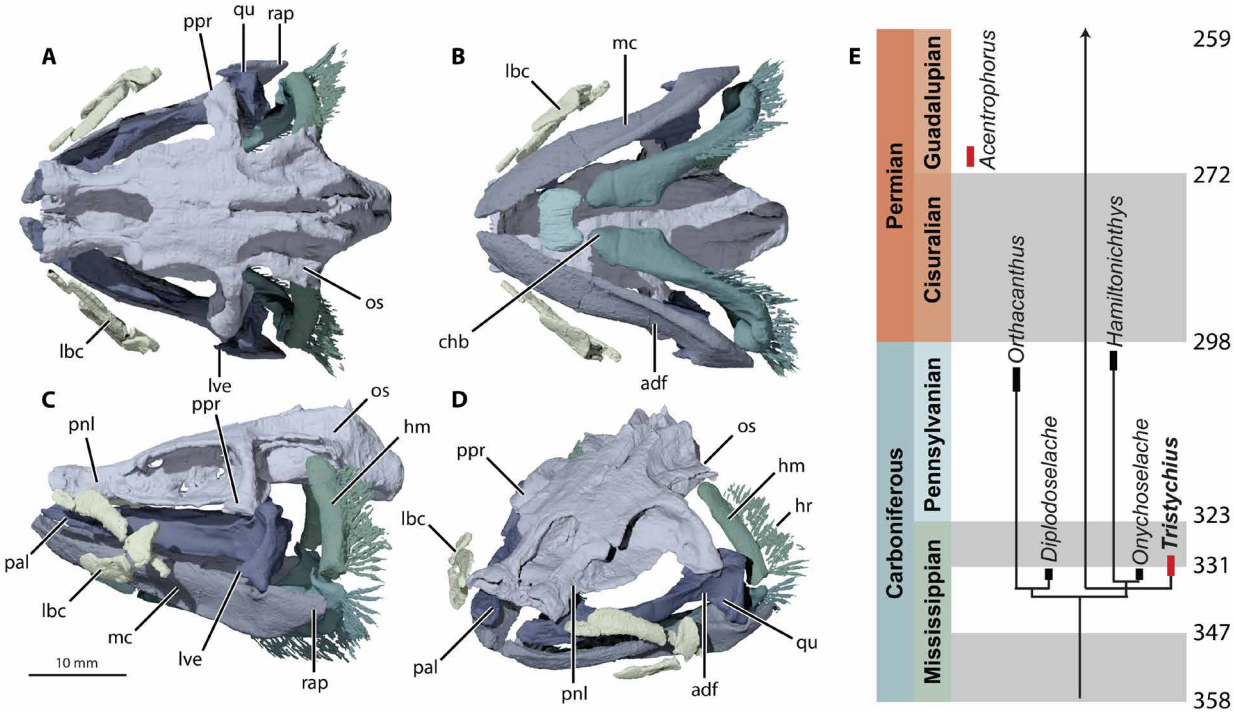

Fig. 1. *T. arcuatus* cranial skeleton. (**A**) Dorsal, (**B**) ventral, (**C**) left lateral, and (**D**) anterior dorsolateral views; contributing specimens in table S1. (**E**) Carboniferous-Permian elasmobranch time-calibrated phylogeny, simplified after (*16*) (boundary ages from Chronostratigraphic Chart ICS V.2018/8); red bars mark earliest gape-limited expanding jaw systems: *Acentrophorus* (*6*), earliest actinopterygian with mobile maxilla. adf, adductor fossa; chb, ceratohyal blade; hm, hyomandibula; hr, hyoid rays; lbc, labial cartilage chain; lve, lateroventral extremity of palatoquadrate; mc, Meckel's cartilage; os, otic shelf; pal, palatine process; pnl, postnasal lamina; ppr, postorbital process; qu, quadrate; rap, retroarticular process.

process. Neither Meckel's cartilage nor the palatoquadrate bears a broad dental groove or furrow associated with the dentition of small (approximately 1.0 mm high) multicuspid teeth (*12*).

Unlike the curved hyomandibulae present in most of the early chondrichthyans (Fig. 2B), the *Tristychius* hyomandibula is short and straight (Fig. 2E and fig. S3, A and B), articulates beneath the rear of the otic shelf (*13*), and extends ventrally and laterally, connecting with the ceratohyal anterior to the level of the occiput. The ceratohyal is massive, relative to the lightly constructed Meckel's cartilage, with a shaft broadening and thickening anteriorly to form a wide, medially directed blade (Fig. 1B and fig. S3, E to H). In ventral view, the ceratohyals frame the insertion of the coracohyoideus muscle. The anterior of each blade articulates with the large basihyal (fig. S3, C and D). Proximally, the ceratohyal shaft turns dorsally and forms a concave platform receiving the distal head of the hyomandibula. The lateral surface of the ascending pillar brackets the retroarticular process of Meckel's cartilage. The hyoid rays are well preserved but, in contrast with previous reconstructions (*8*, *12*), are much too short to form an opercular flap.

The labial cartilages are large and comparable to examples known in Mesozoic hybodontids (*8*) and modern suction feeding elasmobranchs such as nurse sharks (genus *Ginglymostoma*) (*23*). The complete labial chain includes three upper and two lower cartilages (Fig. 1 and fig. S2, I and J). Significantly, the main hinge of the labial chain occurs around the trapezoidal posterior lower cartilage, which bears well-formed articulation surfaces. This hinge is located far to the anterior of the mandibular joint (fig. S4, C and D), thereby limiting the gape aperture laterally and restricting jaw depression (compare Fig. 2, H and I).

The pectoral girdle (fig. S3) is an integral part of the feeding mechanism (*24*). The coracoids are broad, each with a strongly concave posterior surface, likely for accommodating hypaxial trunk musculature (Fig. 2G). The anterior surfaces of left and right sides combined create a wide, shallow pericardial concavity flanked by areas for the origins of coracoarcual and coracohyoideus muscles.

Models and kinematic simulations

The 3D skeletal reconstruction (Fig. 1) derived from these data allowed the assembly of detailed physical (fig. S4) and digital (Fig. 3) models to test the hypothesis that the *Tristychius* cranium was capable of the full range of movements required for specialized suction feeding (*22*). The physical model permits direct investigation of the cranium as an interconnected network of nonplanar, four-bar linkages (fig. S4) (*25*), whereas the digital model (Fig. 3 and figs. S6 and S7) allows multiple conformations of the cartilages, limited only by constraints applied to the articulation surfaces (*25*). In both models, the retroarticular process of Meckel's cartilage is coupled to the ceratohyal. In life, this linkage likely consisted of a set of ligaments (*20*, *21*, *23*). The articulation is pinned in the physical model, but the digital model permits greater flexibility. Notably, in both models, the hyoid bar (ceratohyal and basihyal) is capable of independent rotation.

Both models show that mandibular depression, driven by retraction of the pectoral girdle (*24*), (i) abducts the hyomandibula, (ii) opens and rotates the labial cartilage chain, and (iii) displaces the quadrate laterally across the underside of the postorbital process (fig. S4 and movies S1 to S6). This explains the transverse ridge and groove

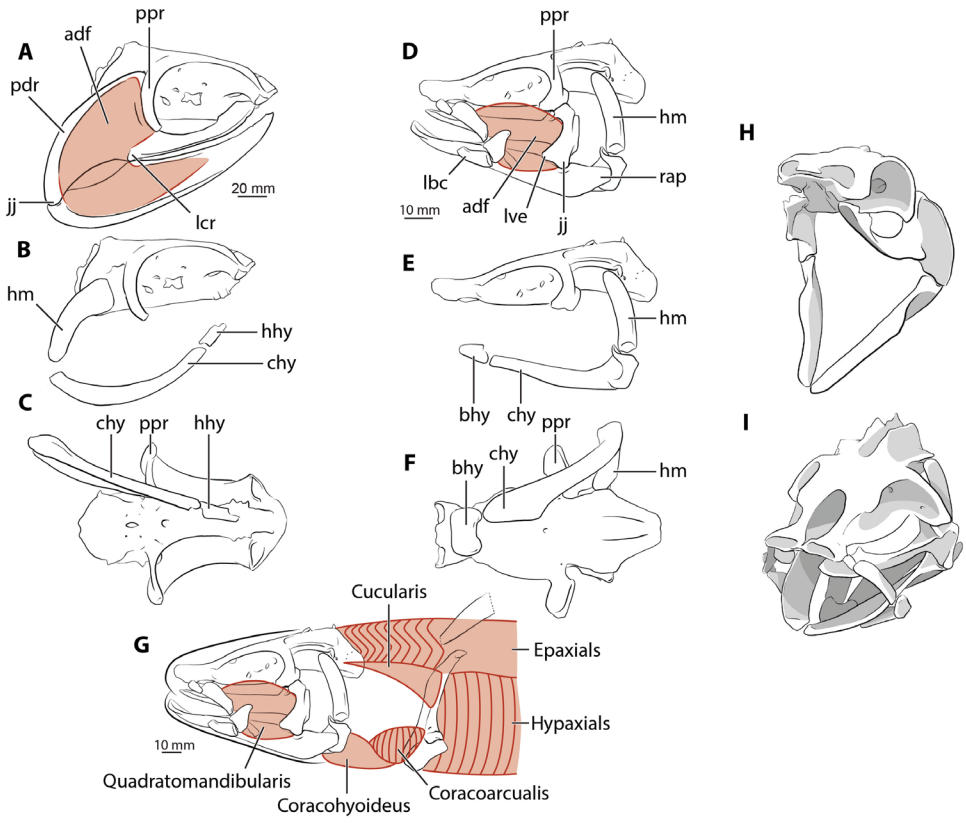

Fig. 2. Symmoriid and *T. arcuatus* crania: contrasting jaw shapes, adductor muscle areas, and hyoid orientations. (**A** to **C**) Symmoriid right lateral view and (**D** to **F**) *Tristychius* left lateral view, neurocranium, hyoid arch, and jaws in articulation. Pink areas indicate estimates of jaw muscle distribution. (**G**) *Tristychius* feeding apparatus (black) and muscles (red) reconstructed; myosepta shown for segmented muscles, adapted from (*24*). (**H**) Symmoriid and (**I**) *Tristychius* crania with jaws open. bhy, basihyal; chy, ceratohyal; hhy, hypohyal; jj, jaw joint; lcr, lateral crest; pdr, posterodorsal rim.

articulation between the quadrate and braincase, long thought to be evidence of enhanced mobility of the palate [J. Dick personal communication (*8*)]. Jaw depression within this 3D linkage network results in a greatly expanded oral cavity with a planar, near-circular mouth aperture (*2*) limited laterally by a skeletally supported rim, similar to the suction feeding motions of white spotted bamboo sharks (*Chiloscyllium plagiosum*) and nurse sharks (*Ginglymostoma cirratum*) (*26*, *27*). The digital model quantifies and coordinates these linked movements within the motion sequence described in Fig. 3: A kinematic simulation validated with reference to motion sequences observed in living taxa (*24*, *26*, *28*), in which expansive and compressive phases of the mandibular arch precede those of the hyoid arch (fig. S7).

The physical model complements the digital model by further allowing direct measurement of oral volume change throughout the motion sequence (Fig. 3A and table S2). Average peak increase in oral volume is 60%. Moreover, half of this additional volume is captured by the expanded cheeks entrained by the labial cartilages. Significantly, although the greatest rate of oral volume increase occurs between mouth closed and maximum depression of Meckel's cartilage, peak oral volume occurs later at maximum depression of the ceratohyal. Thus, as the jaws begin to close, oral cavity expansion continues, maintaining suction throughout the majority of the bite cycle, once again, as in modern sharks and teleosts. The motion sequence in Fig. 3A is plotted as if jaw opening and closing occurred at a constant rate. However, experimental observations show that specialists in suction prey capture actually exhibit a rapid expansive phase (jaw depression) coupled with a slower compressive phase (jaw elevation) (*29*).

DISCUSSION

These results provide unprecedented support for the Chondrichthyes-first conjecture (*2*): *Tristychius* predates the earliest evidence of the nearest equivalent actinopterygian jaw system (*6*) by some 50 million years (Fig. 1). As noted, in *Tristychius*, the labial cartilages function like those of a modern nurse (*22*) or bamboo shark (cf. *Chiloscyllium*; fig. S5) or the free maxilla of fossil (*6*) and modern neopterygians such as a bowfin (*5*) or largemouth bass (*1*). To be effective, the jaws must be brought close to food items before jaw opening because suction dissipates as an inverse function of distance. Thus, high-performance suction mechanisms are advantageous in benthic feeding, as the operational distance can be enhanced if jaws are used close to the substrate boundary (*30*, *31*). For these reasons and consistent with indications from the form of the vestibular labyrinth (*13*) and overall body shape (*12*), we conclude that *Tristychius* was a specialist benthic predator, either ambushing or using stealth to approach its prey.

Ecomorphospace analyses of fishes have generally relied on 2D data (chord lengths or landmark data), gathered in lateral view, to infer ecology (*32*), feeding mechanics (*33*, *34*), and macroevolutionary patterns (*35*, *36*, *37*). This approach is justified for many fish taxa, where the body is laterally compressed (*35*) or movement is restricted

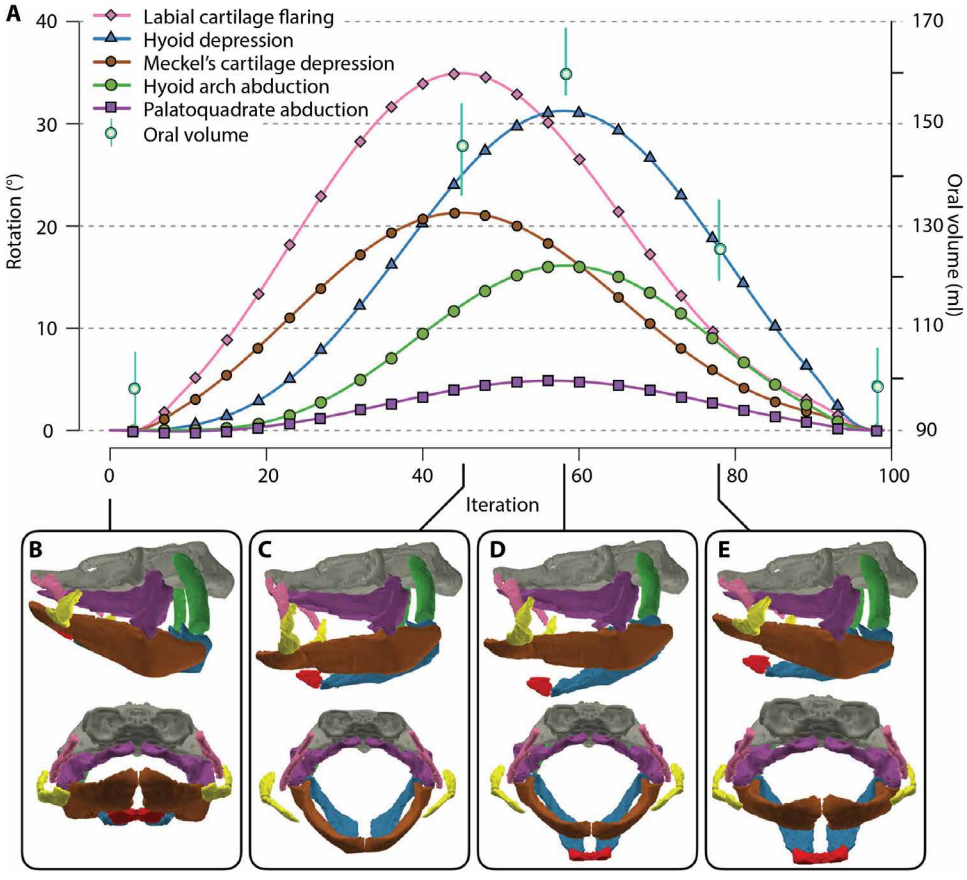

Fig. 3. Mouth opening and closing sequence. (**A**) Reconstructed coordinated cranial cartilage motions and estimates of oral volume through mouth opening and closing cycle. (**B**) Closed mouth. (**C**) Mouth fully open with Meckel's cartilage depressed. (**D**) Mouth closing with hyoid bar fully depressed. (**E**) Mouth closing with hyoid bar elevated. Vertical bars, extending from oral volume estimates, show maximum variance (table S2).

to a single (parasagittal) plane (*34*, *37*). Buser *et al.* (*38*) demonstrated that for sculpins, 2D data often performed as well as 3D data in capturing relevant morphofunctional information. However, as with principal components analysis, 2D data represent compression of a real, complex dataset into a lower dimensionality. Morphological systems involving significant projection into three dimensions or substantial movement orthogonal to the plane of the 2D data can fail to discriminate among different functional morphologies (*39*, *40*). Buser *et al.* (*38*) acknowledged that 2D data failed to perform as well as 3D data for taxa with exaggerated morphologies along their lateral axis.

Demonstration of such an advanced jaw system in *Tristychius* is only possible because of 3D kinematic simulations (*41*), incorporating all parts of the cranial skeleton and integrating multiple lines of evidence. The jaw morphology involves exaggerated lateral projection, and movement on jaw opening involves significant lateral displacement. If analyzed using chord measurements taken in lateral view as a proxy for mandibular shape disparity (*36*), then *Tristychius* is reconstructed as a rather unexceptional chondrichthyan (fig. S8 and table S3). Therefore, this pivotal evolutionary transition from a feeding mechanism relying primarily on biting and ram feeding (*31*) to one that exploits suction through rapid oral cavity expansion (Fig. 2) is invisible in this analytical treatment. Hence, the paleoecological implications of an advanced high-performance suction feeding system in *Tristychius* would be lost.

These data present an exception to widely accepted assumptions of chondrichthyan evolutionary conservatism, exemplifying the evolvability of the elasmobranch feeding apparatus (*22*). Furthermore, these derived jaws signal elasmobranch expansion into novel niche space, and perhaps increased prey selectivity (*31*), in the aftermath of the end-Devonian extinctions (*10*). Accordingly, *Tristychius* marks the emergence of a new ecological guild of jawed vertebrates (*42*): a morphofunctionally modern fish (fig. S9) deep within the Paleozoic. This mode of suction feeding, foreshadowing its use by the vast majority of living fishes (*1*, *2*), implies an enhanced ability to capture cryptic and/or elusive prey (movie S6). Now vulnerable to vertebrate predators with a battery of sensory systems (*31*), infaunal prey taking shallow refuge in crevices or benthic sediments seem likely to have been pressured into deeper burrows. Furthermore, this new mode of feeding might have exerted a devastating impact on fish nursery grounds, often located in shallow brackish environments (*43*), such as the Wardie Beach paleoenvironment. The emergence of fishes such as *Tristychius* likely resulted in a fundamental shift in predator-prey dynamics (*44*, *45*), the bulk effects of which might yet be detected in the sedimentary record.

Tristychius is by far the most abundant shark in collections from Wardie Beach (*14*), but, as with the origin of actinopterygian jaw protrusion (*44*), this first appearance of enhanced suction feeding does not appear to have triggered an evolutionary radiation. Rather, *Tristychius* emerged from within an exceptional round of chondrichthyan

morphological diversification following the end-Devonian extinction (*10*) and likely initiated the evolution of increasingly kinetic and diverse crania among the elasmobranchs, standing in marked contrast to the anatomically conservative jaws and tooth plates of their holocephalan sister taxon.

MATERIALS AND METHODS

Geological setting and material

The Wardie Shales represent a Member of the Gullane Formation, part of the West Lothian, Viséan stage Strathclyde Group (*32*–*35*, *46*, *47*). The minimum age constraint for the Wardie Shales Member is defined by the nodosa conodont zone at the base of the Brigantian substage: no less than 333.95 ± 0.39 Ma (*48*). This overlies the Asbian substage MacGregor Marine Band goniatites from zone B2 of the English succession (*37*, *38*, *49*–*52*), which, in turn, overlie the Wardie Shales. The maximum age constraint for the Gullane Formation is provided by the underlying Arthur's Seat Volcanic Formation, $^{40}Ar/^{39}Ar$ dating of which is 335.1 ± 0.6 Ma (*53*). It follows that the age of the Wardie Shales Member is restricted to between ~333.5 and 335.5 Ma (*54*).

The Oil Shales of the Midland Valley of Scotland, including the Wardie Shale Member, were deposited on the floor of a large and likely thermally stratified lagoon, stagnant parts of which permitted chondrichthyan skeletal preservation (*15*, *55*–*58*). Irrespective of evidence of occasional marine influence, the shark component of the fossil biota, which also includes brachiopods, bivalves, ostracods, actinopterygians, and sarcopterygians including the tetrapod *Lethiscus* (*59*), persists throughout six of seven fish-bearing beds at Wardie shore. Hence, it appears that these Oil Shale sharks (*12*, *15*, *55*), of which *T. arcuatus* is by far the most abundant (*14*), were either nonmarine or able to tolerate a wide range of salinities.

Concretions (nodules) (fig. S1A) are restricted to the fish-bearing beds. Skeletal remains embedded within siderite matrix are often surrounded by a halo of iron pyrite and calcite-filled radiating cracks (*14*, *15*). Preserved shark cartilage is occasionally freed from the surrounding matrix, but these items often consist of the cartilage core, with calcified tesserae and surface detail remaining embedded in the concretion. For this reason, mechanical preparation of specimens is not recommended, and nondestructive methods, such as computed tomography, are preferred.

Computed tomography

Concretions containing *T. arcuatus* were scanned at the University of Texas at Austin (www.digimorph.org) high-resolution x-ray computed tomography facility. Sixteen-bit TIFF (Tagged Image File Format) images (1024 by 1024 pixels) were obtained using P250D, 450 kV, 1.3 mA, a small spot size, 1 brass filter, no offset, and gain used in lieu of wedge [integration time, 128 ms; slice thickness, 0.25 mm; S.O.D. (Source to Object Distance), 582 mm, 1000 views, 1 ray per view, 1 sample per view; interslice spacing, 0.23 mm; field of reconstruction, around 120 mm (maximum field of view, 120.8318 mm); reconstruction offset, 12,000; reconstruction scale, 4800]. Ring-removal processing was completed on the basis of the correction of raw sinogram data using IDL (Interactive Data Language) routine "RK_SinoRingProcSimul" with parameter "sectors = 100." Postreconstruction ring correction used parameters "oversample = 2, binwidth = 21, sectors = 1."

The bamboo shark, *Chiloscyllium punctatum* (snout to tail length, 120 mm) was stained in phosphotungstic acid in ethanol (1% solution) for 2 weeks. Scans were completed at the University of Chicago X-ray Computed Tomography facility, using a GE Phoenix 240/180 scanner at 75 kV and 150 μA, with no filter, and 1600 projections with a voxel size of 13.90 μm.

Rendering and reconstructions

Anatomical reconstructions of *T. arcuatus* used Mimics v.18 (http://biomedical.materialise.com/mimics; Materialise, Leuven, Belgium) for 3D modeling, including segmentation, 3D object rendering, STL (Stereo Lithography) polygon creation, and kinematics. Further editing of the STLs (color, texture, and lighting), kinematics, and mirroring for the final restoration used 3D Studio Max (www.autodesk.com/products/3ds-max/overview; Autodesk, San Rafael, USA). All specimens listed in table S1 were used for corroboration of cartilage morphology preserved with different patterns of postmortem compression and for scaling the complete cranial skeleton.

The model symmoriid in Fig. 2 (A to C and H) is a composite assembled using the 3D intact neurocranium of *Dwykaselachus* (*60*) and the mandibular and hyoid arches of *Akmonistion* (*61*), with input on articulation and orientation from *Ozarcus* (*18*). The *Dwykaselachus* neurocranium most closely resembles the flattened remains of *Akmonistion* neurocrania; hence, the use of jaws and hyoid arch from *Akmonistion* (specimen V8246 from University of Glasgow Hunterian Museum, specimen GN1047 from University of Cambridge Museum of Zoology, and specimen 1981.63.23A from National Museum of Scotland) rescaled to fit *Dwykaselachus*. Neurocranial articular surfaces match those of *Ozarcus*, but it is clear that the palate proportions differ from *Akmonistion*. Data from the Permian xenacanth *Orthacanthus* (*8*, *62*) might be used similarly, also displaying cleaver-shaped jaws (*19*), but no ventral perspective of arches in articulation with braincase is available, unlike published images of *Ozarcus*.

The physical model of *Tristychius* shown in fig. S4 was assembled from life-sized 3D printouts of the STL files for 3D object rendering. All articulations are threaded with steel wire, except for a nylon fiber ligament connecting the hyomandibula to the ceratohyal. The postorbital process–quadrate articulation is free, held in position by the rest of the jaw suspension. Tension in the model can be maintained by a sprung brace inserted between the quadrates, thereby keeping the gape open (fig. S4F).

Virtual simulation methods

To virtually simulate mouth opening and closing in *T. arcuatus*, we first arranged the computed tomography segmented skeletal elements (i.e., digital meshes) in an approximately closed mouth pose. On the basis of the articular anatomy of *T. arcuatus* and the cranial mechanics and kinematics of present-day sharks (*63*), we concluded that the skull of *T. arcuatus* likely had at least six primary degrees of freedom (DoFs) of motion (fig. S6). These are translation of the basihyal dorsoventrally and craniocaudally (fig. S6, A and B), hyoid arch abduction (fig. S6C), Meckel's cartilage depression (fig. S6D), mandibular arch abduction (fig. S6E), and labial cartilage flaring (fig. S6F).

Given these multiple DoFs, many potential conformations of the skull are possible. Thus, we simulated a single sequence of opening and closing of the mouth by charting a single path or trajectory through this multidimensional "skull conformation space." We created an initial 5D skull conformation space by simulating motion along five of six cranial DoFs (all but labial cartilage flaring): The basihyal was translated ventrally over a range of 35 mm and caudally over a range of 10 mm, the hyoid arch was abducted over a range of 25°, the Meckel's cartilage was depressed over a range of 20°, and the

mandibular arch was abducted over a range of 5° (we assumed bilateral symmetry throughout all virtual simulation). For each of these motions, we simulated nine positions evenly spaced along the total range of motion and combined them in a full pairwise manner, creating a total of 9^5 (59,049) conformations. We performed all simulations in R (*64*), using the R package "linkR" to perform the motion transformations (*65*, *66*) and the R package "svgViewR" (*67*) to create all mesh visualizations and animations (movies S1 to S5).

Not all of these conformations are biologically reasonable or biomechanically feasible. We next filtered out these conformations based on two criteria. The first criterion was that when the Meckel's cartilage is near fully depressed, the basihyal would not be near fully elevated and that when the basihyal was near fully depressed, the Meckel's cartilage would not be near fully elevated (fig. S7A). This follows from the assumption that during prey capture mandibular and hyoid arch rotations are coordinated (although not necessarily synchronous). This first criterion reduced the number of conformations from 59,049 to 22,491.

The second filtering criterion assumed the presence of a ligamentous connection between the medial surface of the retroarticular process of the Meckel's cartilage and the opposing lateral surface at the proximal (caudal) end of the ceratohyal. We removed conformations in which the distance between these two surfaces exceeded 4 mm by taking the distance between two planes, one on each articular surface. Because we simulated hyoid arch abduction (fig. S6C) independently of basihyal translation (fig. S6, A and B) and mandibular arch rotations (fig. S6, D and E), for some conformations, the hyoid arch and mandibular arch meshes penetrated (i.e., intersected) each other (fig. S7B). We also removed these conformations by detecting intersections of the two articular planes. This second criterion reduced the number of conformations from 22,491 to 1042.

We next defined a trajectory curve through the filtered conformation space (1042 total conformations) that represents a possible mouth opening-closing motion sequence (red lines in fig. S7, C to E) validated by reference to in vivo kinematics described in present-day sharks (*7*, *22*–*24*, *63*). In particular, we defined the trajectory through conformation space such that peak hyoid depression follows peak Meckel's cartilage depression (fig. S7C). In addition, we conjectured that mandibular arch abduction (i.e., palatoquadrate mediolateral sliding; fig. S7D) and hyoid arch abduction (fig. S7E) both reached their respective maxima at peak hyoid depression. To constrain the trajectory curve (e.g., make sure the path passes through particular points), we used Bézier splines. We then found the points in conformation space closest to evenly spaced points along the motion trajectory and smoothed the transformations between consecutive conformations to create the final mouth open-close simulation. Labial cartilage flaring was added last and with the assumption that flaring occurs simultaneous with Meckel's cartilage depression. Thus, the labial cartilage transformation was essentially a copy of Meckel's cartilage depression, rescaled to a maximum of 35°.

Estimates of oral volume change through bite cycle

Measures of oral volume were obtained from direct fills of the physical model (fig. S4). The model was supported, occiput uppermost, with the oral cavity lined with a plastic bag. Meckel's cartilage and the ceratohyal (and basihyal) were rotated to angles recorded in Fig. 3A and table S2, with associated abduction or adduction of the hyomandibula and palatoquadrate. Arch positions were secured using a wire cage. At each fixed position, the oral cavity (plastic lined) was filled to the level of hyoceratohyal joint with charcoal pellets decanted from a measuring cylinder. Although positions of articulated skull parts were fixed, the cheek and throat walls were flexible, as they must have been in life. Thus, measurements of oral volume varied for each fixed position. For this reason, 10 measurements were taken for each of the four configurations of the feeding apparatus, obtained throughout the mouth opening and closing cycle. The extra oral volume captured by the labial cartilages was measured from a wedge-shaped container built to fit the space extending from the jaw hinge (the quadrate-articular joint) to the level of the oral rim bordered by the labial cartilages when Meckel's cartilage is fully depressed.

2D mandible morphometrics

Previous studies of mandibular morphological disparity have treated the mandible as a 2D object examined in lateral view (*36*, *37*). These treatments can identify changes in mandible shape through time and across clades, and given the close association of mandibular form and feeding ecology, it is reasonable to infer expansion into novel ecological niches when novel mandible morphologies are observed.

The mandible in "fishes" is generally amenable to representation as a 2D object. However, compression of any 3D object into 2D necessarily loses any information along the axis orthogonal to the plane of analysis. This compression is not necessarily fatal to morphometric analyses (*38*); however, in cases where there is significant shape disparity along the orthogonal axis, there will be increasing bias in the results (*38*, *40*).

In the case of the mandible, the compressed axis projects laterally from the sagittal plane of the neurocranium. It is precisely in this plane that the displacement of the palatoquadrate and the abduction of the hyomandibula in *Tristychius* takes place during the jaw-opening phase, with most of the increase in oral volume being a result of lateral expansion of the cheeks. Hence, methods, such as those used by Anderson *et al.* (*36*) or Hill *et al.* (*37*), would be unable to recover the unique nature of the jaws in *Tristychius*. By way of demonstration, we coded three chord measurement characters defining anterior (C1) and posterior (C2) mechanical advantage and mandible beam strength (C3) for *Tristychius* and other Devonian and Carboniferous chondrichthyan taxa, using the measurements specified by Anderson *et al.* (*36*). Plotting these chondrichthyan taxa along with the original data from Anderson *et al.* (*36*) demonstrates that none of these new taxa (including *Tristychius*) are outliers (fig. S8, A and B); all are clustered in a group with other chondrichthyans. Hence, the novel morphology observed in *Tristychius*, and its inferred novel ecological niche, would be lost in a large-scale macroevolutionary analysis based on a 2D representation of this taxon.

SUPPLEMENTARY MATERIALS

Supplementary material for this article is available at http://advances.sciencemag.org/cgi/content/full/5/9/eaax2742/DC1

Fig. S1. *Tristychius arcuatus*, renderings of key specimens.
Fig. S2. Mandibular arch cartilages of *T. arcuatus*.
Fig. S3. Hyoid arch and pectoral girdle of *T. arcuatus*.
Fig. S4. *T. arcuatus*: physical model showing interconnected 3D four-bar linkages.
Fig. S5. The cranial skeleton of a juvenile *Chiloscyllium punctatum* reconstructed from high-resolution computed tomography.
Fig. S6. Conformations of the skull of *T. arcuatus*.
Fig. S7. Filtering the dataset of *T. arcuatus* cranial conformations.
Fig. S8. Morphospace for early gnathostomes relative to jaw measurement characters from Anderson *et al.* (*36*).
Fig. S9. Life restoration of *T. arcuatus* from the Viséan Wardie Shales of Edinburgh, Scotland.
Table S1. *T. arcuatus* specimens contributing to study.

Table S2. Measurements of oral volume (milliliters) from physical model of *T. arcuatus*.
Table S3. Additions to Anderson *et al.* (*36*) dataset of mandible metrics.
Movie S1. Jaw and hyoid motion sequences modeled in caudal view.
Movie S2. Jaw and hyoid motion sequences modeled in cranial view.
Movie S3. Jaw and hyoid motion sequences modeled in dorsal view.
Movie S4. Jaw and hyoid motion sequences modeled in lateral view.
Movie S5. Jaw and hyoid motion sequences modeled in ventral view.
Movie S6. Animation of complete cranial to pectoral skeleton opening and closing jaws, ingesting prey.
References (*68*–*77*)

REFERENCES AND NOTES

1. A. L. Camp, T. J. Roberts, E. L. Brainerd, Swimming muscles power suction feeding in largemouth bass. *Proc. Natl. Acad. Sci.* **112**, 8690–8695 (2015).
2. P. C. Wainwright, M. D. McGee, S. J. Longo, L. P. Hernandez, Origins, innovations, and diversification of suction feeding in vertebrates. *Integr. Comp. Biol.* **55**, 134–145 (2015).
3. P. J. Motta, C. D. Wilga, Advances in the study of feeding behaviors, mechanisms, and mechanics of sharks. *Environ. Biol. Fish* **60**, 131–156 (2001).
4. G. V. Lauder, K. F. Liem, The evolution and interrelationships of actinopterygian fishes. *Bull. Mus. Comp. Zool.* **150**, 95–197 (1983).
5. M. Benton, *Vertebrate Palaeontology* (Wiley Blackwell, ed. 4, 2015).
6. E. L. Gill, The permian fishes of the genus *acentrophorus*. *Proc. Zool. Soc.* **93**, 19–40 (1923).
7. E. H. Wu, Kinematic analysis of jaw protrusion in orectolobiform sharks: A new mechanism for jaw protrusion in elasmobranchs. *J. Morphol.* **222**, 175–190 (1994).
8. J. G. Maisey, The postorbital palatoquadrate articulation in elasmobranchs. *J. Morphol.* **269**, 1022–1040 (2008).
9. E. D. Grogan, R. Lund, *Debeerius ellefseni* (Fam. Nov., Gen. Nov., Spec. Nov.) an autodiastylic chondrichthyan from the Mississippian Bear Gulch Limestone of Montana (USA), the relationships of the Chondrichthyes, and comments on gnathostome evolution. *J. Morphol.* **243**, 219–245 (2000).
10. M. Friedman, L. Cole Sallan, Five hundred million years of extinction and recovery: A phanerozoic survey of large-scale diversity patterns in fishes. *Palaeontology* **55**, 707–742 (2012).
11. L. Agassiz, *Recherches sur les poissons fossiles* (Petitpierre, 1837), vol. 3.
12. J. R. F. Dick, On the carboniferous shark *Tristychius arcuatus* Agassiz from Scotland. *Earth Env. Sci. Trans. R. Soc. Edinb.* **70**, 63–108 (1978).
13. M. I. Coates, K. Tietjen, The neurocranium of the lower carboniferous shark *Tristychius arcuatus* (Agassiz, 1837). *Earth Env. Sci. Trans. R. Soc. Edinb.* **108**, 19–35 (2018).
14. S. P. Wood, Recent discoveries of Carboniferous fishes in Edinburgh. *Scot. J. Geol.* **11**, 251–258 (1975).
15. D. L. Dinely, S. J. Metcalf, *Fossil Fishes of Great Britain* (Geological Conservation Review Series, Joint Nature Conservation Committee, 1999), vol. 16.
16. M. I. Coates, J. A. Finarelli, I. J. Sansom, P. S. Andreev, K. E. Criswell, K. Tietjen, M. L. Rivers, P. J. La Riviere, An early chondrichthyan and the evolutionary assembly of a shark body plan. *Proc. Biol.Sci.* **285**, 20172418 (2018).
17. A. Pradel, P. Tafforeau, J. G. Maisey, P. A. Janvier, A new paleozoic symmoriiformes (Chondrichthyes) from the late carboniferous of Kansas (USA) and cladistic analysis of early chondrichthyans. *PLOS ONE* **6**, e24938 (2011).
18. A. Pradel, J. G. Maisey, P. Tafforeau, R. H. Mapes, J. Mallatt, A Palaeozoic shark with osteichthyan-like branchial arches. *Nature* **509**, 608–611 (2014).
19. B. Schaeffer, Comments on the origin and basic radiation of the gnathostome fishes with particular reference to the feeding mechanism, in *Problèmes Actuels De Paléontologie: Évolution Des Vertébrés* (Colloques internationaux du Centre national de la Recherche scientifique 218 Paris, 1975), pp. 101–109.
20. S. A. Moss, The feeding mechanism of sharks of the family Carcharhinidae. *J. Zool.* **167**, 423–436 (1972).
21. P. J. Motta, C. A. D. Wilga, Anatomy of the feeding apparatus of the lemon shark, *Negaprion brevirostris*. *J. Morphol.* **226**, 309–329 (1995).
22. P. J. Motta, D. R. Huber, Prey capture behavior and feeding mechanisms of elasmobranchs, in *Biology of Sharks and Their Relatives*, J. Musick, J. Carrier, M. Heithaus, Eds. (CRC Press, 2012), pp. 153–209.
23. P. J. Motta, R. E. Hueter, T. C. Tricas, A. P. Summers, D. R. Huber, D. Lowry, K. R. Mara, M. P. Matott, L. B. Whitenack, A. P. Wintzer, Functional morphology of the feeding apparatus, feeding constraints, and suction performance in the nurse shark *Ginglymostoma cirratum*. *J. Morphol.* **269**, 1041–1055 (2008).
24. A. L. Camp, B. Scott, E. L. Brainerd, C. D. Wilga, Dual function of the pectoral girdle for feeding and locomotion in white-spotted bamboo sharks. *Proc. Biol. Sci.* **284**, 20170847 (2017).
25. A. M. Olsen, A. L. Camp, E. L. Brainerd, The opercular mouth-opening mechanism of largemouth bass functions as a 3D four-bar linkage with three degrees of freedom. *J. Exp. Biol.* **220**, 4612–4623 (2017).
26. C. D. Wilga, L. A. Ferry, Functional anatomy and biomechanics of the feeding apparatus, in *Physiology of Elasmobranch Fishes: Structure and Interaction with Environment*, R. E. Shadwick, A. P. Farrell, C. J. Brauner, Eds. (Academic Press, 2016), vol. 34A, pp. 153–187.
27. P. J. Motta, C. A. D. Wilga, Anatomy of the feeding apparatus of the nurse shark, *Ginglymostoma cirratum*. *J. Morphol.* **241**, 33–60 (1999).
28. T. Kleinteich, J. Herzen, F. Beckmann, M. Matsui, A. Haas, Anatomy, function, and evolution of jaw and hypobranchial muscles in cryptobranchoid salamander larvae. *J. Morphol.* **275**, 230–246 (2014).
29. P. J. Motta, R. E. Hueter, T. C. Tricas, A. P. Summers, Kinematic analysis of suction feeding in the nurse shark *Ginglymostoma cirratum* (Orectolobiformes, Ginglymostomatidae). *Copeia* **2002**, 24–38 (2002).
30. L. A. Ferry, E. M. Paig-Tran, A. C. Gibb, Suction, ram, and biting: Deviations and limitations to the capture of aquatic prey. *Integr. Comp. Biol.* **55**, 97–109 (2015).
31. D. Huber, C. Wilga, M. Dean, L. Ferry, J. Gardiner, L. Habegger, Y. Papastamatiou, J. Ramsay, L. Whitenack, Feeding in cartilaginous fishes: An interdisciplinary synthesis, in *Feeding in Vertebrates,* V. Bels, I. Q. Whishaw, Eds. (Springer Nature, 2019) pp. 231–295.
32. D. C. Collar, P. C. Wainwright, Discordance between morphological and mechanical diversity in the feeding mechanism of centrarchid fishes. *Evolution* **60**, 2575–2584 (2006).
33. P. S. L. Anderson, M. W. Westneat, A biomechanical model of feeding kinematics for *Dunkleosteus terrelli* (Arthrodira, Placodermi). *BioOne* **35**, 251–269 (2009).
34. J. R. Grubich, M. W. Westneat, Four-bar linkage modelling in teleost pharyngeal jaws: Computer simulations of bite kinetics. *J. Anat.* **209**, 79–92 (2006).
35. L. C. Sallan, M. Friedman, Heads or tails: Staged diversification in vertebrate evolutionary radiations. *Proc. Biol. Sci.* **279**, 2025–2032 (2012).
36. P. S. Anderson, M. Friedman, M. D. Brazeau, E. J. Rayfield, Initial radiation of jaws demonstrated stability despite faunal and environmental change. *Nature* **476**, 206–209 (2011).
37. J. E. Hill, M. N. Puttick, T. L. Stubbs, E. J. Rayfield, P. J. Donoghue, Evolution of jaw disparity in fishes. *Palaeontology* **61**, 847–854 (2018).
38. T. J. Buser, B. L. Sidlauskas, A. P. Summers, 2D or not 2D? Testing the utility of 2D vs 3D landmark data in geometric morphometrics of the sculpin subfamily Oligocottinae (Pisces; Cottoidea). *Anat. Rec.* **301**, 806–818 (2018).
39. M. R. G. Attard, E. Sherratt, P. McDonald, I. Young, M. Vidal-García, S. Wroe, A new, three-dimensional geometric morphometric approach to assess egg shape. *PeerJ* **6**, e5052 (2018).
40. M. J. Hopkins, J. K. Pearson, Non-linear ontogenetic shape change in *Cryptolithus tesselatus* (Trilobita) using three-dimensional geometric morphometrics. *Palaeontol. Electron.* **19.3.42A**, 1–54 (2016).
41. J. A. Nyakatura, K. Melo, T. Horvat, K. Karakasiliotis, V. R. Allen, A. Andikfar, E. Andrada, P. Arnold, J. Lauströer, J. R. Hutchinson, M. S. Fischer, A. J. Ijspeert, Reverse-engineering the locomotion of a stem amniote. *Nature* **565**, 351–355 (2019).
42. D. Simberloff, T. Dayan, The guild concept and the structure of ecological communities. *Annu. Rev. Ecol. Syst.* **22**, 115–143 (1991).
43. L. Cole Sallan, M. I. Coates, The long-rostrumed elasmobranch *Bandringa* Zangerl, 1969, and taphonomy within a Carboniferous shark nursery. *J. Vertebr. Paleontol.* **34**, 22–33 (2014).
44. P. W. Signore, C. E. Brett, The Mid-Paleozoic precursor to the Mesozoic marine revolution. *Paleobiology* **10**, 229–245 (1984).
45. D. R. Bellwood, C. H. R. Goatley, O. Bellwood, D. J. Delbarre, M. Friedman, The rise of jaw protrusion in spiny-rayed fishes closes the gap on elusive prey. *Curr. Biol.* **25**, 2696–2700 (2015).
46. J. I. Chisholm, A. D. McAdam, P. J. Brand, "Lithostratigraphical classification of Upper Devonian and Lower Carboniferous rocks in the Lothians" (Technical Report WA/89/26, British Geological Survey, 1989).
47. J. I. Chisholm, P. J. Brand, Revision of the late Dinantian sequence in Edinburgh and West Lothian. *Scot. J. Geol.* **30**, 97–104 (1994).
48. V. I. Davydov, D. Korn, M. D. Schmitz, The carboniferous period, in *The Geologic Time Scale 2012,* F. Gradstein, J. Ogg, M. D. Schmitz, G. Ogg, Eds. (Elsevier, 2012), vol. 1, pp. 603–651.
49. C. N. Waters, M. A. E. Browne, N. S. Jones, I. D. Somerville, Midland valley of Scotland, in *A Revised Correlation of Carboniferous Rocks in the British Isles* (Geological Society, 2011), vol. 26, pp. 96–102.
50. C. N. Waters, I. D. Somerville, M. H. Stephenson, C. J. Cleal, S. L. Long, Biostratigraphy, in *A Revised Correlation of Carboniferous Rocks in the British Isles* (Geological Society, 2011), vol. 26, pp. 1–22.
51. E. D. Currie, XIV—Scottish Carboniferous goniatites. *Trans R. Soc. Edinb.* **62**, 527–602 (1954).
52. R. B. Wilson, A study of the Dinantian marine macrofossils of central Scotland. *Trans R. Soc. Edinb.* **80**, 91–126 (1989).
53. A. A. Monoghan, M. A. E. Browne, D. N. Barford, An improved chronology for the Arthur's Seat volcano and Carboniferous magmatism of the Midland Valley of Scotland. *Scot. J. Geol.* **50**, 165–172 (2014).

54. M. Friedman, S. E. Pierce, M. I. Coates, S. Giles, Feeding structures in the ray-finned fish *Eurynotus crenatus* (Actinopterygii: Eurynotiformes): Implications for trophic diversification among Carboniferous actinopterygians. *Earth Env. Sci. Trans. R. Soc. Edinb.* **109**, 33–47 (2019).
55. J. R. F. Dick, *Diplodoselache woodi* gen. et sp. nov., an early Carboniferous shark from the Midland Valley of Scotland. *Trans R. Soc. Edinb.* **72**, 99–113 (1981).
56. J. T. Greensmith, Rhythmic deposition in the Carboniferous Oil-Shale Group of Scotland. *J. Geol.* **70**, 355–364 (1962).
57. J. T. Greensmith, Calciferous sandstone sedimentation at the eastern end of the midland valley of Scotland. *J. Sediment. Petrol.* **35**, 223–242 (1965).
58. S. P. Hesselbo, N. H. Trewin, Deposition, diagenesis and structures of the Cheese Bay Shrimp bed, Lower Carboniferous, East Lothian. *Scott. J. Geol.* **20**, 281–296 (1984).
59. J. D. Pardo, M. Szostakiwskyj, P. E. Ahlberg, J. S. Anderson, Hidden morphological diversity among early tetrapods. *Nature* **546**, 642–645 (2017).
60. M. I. Coates, R. W. Gess, J. A. Finarelli, K. E. Criswell, K. Tietjen, A symmoriiform chondrichthyan braincase and the origin of chimaeroid fishes. *Nature* **541**, 208–211 (2017).
61. M. I. Coates, S. E. K. Sequeira, A new stethacanthid chondrichthyan from the Lower Carboniferous of Bearsden, Scotland. *J. Vertebr. Paleontol.* **21**, 438–459 (2001).
62. N. Hotton, Jaws and teeth of American xenacanth sharks. *J. Paleontol.* **26**, 489–500 (1952).
63. C. D. Wilga, C. P. Sanford, Suction generation in white-spotted bamboo sharks *Chiloscyllium plagiosum*. *J. Exp. Biol.* **211**, 3128–3138 (2008).
64. R Core Team, *R: A Language and Environment for Statistical Computing* (2018); www.R-project.org/.
65. A. M. Olsen, M. W. Westneat, Linkage mechanisms in the vertebrate skull: Structure and function of three-dimensional, parallel transmission systems. *J. Morphol.* **277**, 1570–1583 (2016).
66. A. M. Olsen, *linkR: 3D Lever and Linkage Mechanism Modeling* (2017); http://cran.r-project.org/package=linkR.
67. A. M. Olsen, *svgViewR: 3D Animated Interactive Visualizations Using SVG* (2018); http://cran.r-project.org/package=svgViewR.
68. G. C. Young, Devonian sharks from south-eastern Australia and Antarctica. *Palaeontology* **54**, 991–1008 (1982).
69. R. Zangerl, G. R. Case, *Cobelodus aculeatus* (Cope), an anacanthous shark from Pennsylvanian black shales of North America. *Palaeontographica A* **154**, 107–157 (1976).
70. R. Lund, On *Damocles serratus,* nov. gen. et sp. (Elasmobranchii: Cladodontida) from the Upper Mississippian Bear Gulch Limestone of Montana. *J. Vertebr. Paleontol.* **6**, 12–19 (1986).
71. R. Lund, The morphology of *Falcatus falcatus* (St. John and Worthen), a Mississippian stethacanthid chondrichthyan from the Bear Gulch Limestone of Montana. *J. Vertebr. Paleontol.* **5**, 1–19 (1985).
72. J. A. Long, C. J. Burrow, M. Ginter, J. Maisey, K. M. Trinajstic, M. I. Coates, G. C. Young, T. J. Senden, First shark from the Late Devonian (Frasnian) Gogo Formation, Western Australia sheds new light on the development of tessellated calcified cartilage. *PLOS ONE* **10**, e0126066 (2015).
73. L. Tapinala, J. Pruitt, A. Pradel, C. D. Wilga, J. B. Ramsay, R. Schlader, D. A. Didier, Jaws for a spiral-tooth whorl: CT images reveal novel adaptation and phylogeny in fossil *Helicoprion*. *Biol. Lett.* **9**, 20130057 (2013).
74. A. Pradel, Skull and brain anatomy of Late Carboniferous Sibyrhynchidae (Chondrichthyes, Iniopterygia) from Kansas and Oklahoma (USA). *Geodiversitas* **32**, 595–661 (2010).
75. E. D. Grogan, R. Lund, A basal elasmobranch, *Thrinacoselache gracia* n. gen and sp., (Thrinacodontidae, new family) from the Bear Gulch limestone, Serpukhovian of Montana, USA. *J. Vertebr. Paleontol.* **28**, 970–988 (2008).
76. U. H. J. Heidtke, C. Schwind, K. Krätschmer, Über die Organisation des Skelettes und die verwandschaftlichen Beziehungen der Gattung *Triodus* Jordan 1849 (Elasmobranchii: Xenacanthida). *Mainzer geowiss. Mitt.* **32**, 9–54 (2004).
77. J. A. Lane, J. G. Maisey, Pectoral anatomy of *Tribodus limae* (Elasmobranchii: Hybodontiformes) from the Lower Cretaceous of northeastern Brazil. *J. Vertebr. Paleontol.* **29**, 25–38 (2009).

Acknowledgments: We thank J. Maisano and the High-Resolution X-ray Computed Tomography facility at the University of Texas at Austin; S. Walsh and N. Fraser, National Museum of Scotland, for loan of specimens; K. Criswell for advice on staining protocols; J. Dick for discussion and unpublished Ph.D. thesis notes. **Funding:** The study was supported by NSF (USA) grants DEB-0917922 and DEB-1541491 (to M.I.C.) and DEB-1612230 (to A.M.O.).
Author contributions: M.I.C. conceived the project, further developed with J.A.F., K.T., and A.M.O. K.T. scanned *Chiloscyllium*, segmented the computer tomography data, and prepared graphics. A.M.O. completed computer 3D-simulated motion analyses. M.I.C. completed physical model motion analyses. J.A.F. completed morphometric analyses. M.I.C. and J.A.F. wrote the manuscript with input from A.M.O. and K.T. **Competing interests:** The authors declare that they have no competing interests. **Data and materials availability:** All data needed to evaluate the conclusions in the paper are present in the paper and/or the Supplementary Materials. Additional data related to this paper may be requested from the authors. All specimens are accessioned at and have been returned to the National Museum of Scotland, Edinburgh, UK. Datasets will be available via Phenome10K (http://phenome10k.org/).

Submitted 8 March 2019
Accepted 9 August 2019
Published 11 September 2019
10.1126/sciadv.aax2742

Citation: M. I. Coates, K. Tietjen, A. M. Olsen, J. A. Finarelli, High-performance suction feeding in an early elasmobranch. *Sci. Adv.* **5**, eaax2742 (2019).